ACS OMEGA

Open Access

http://pubs.acs.org/journal/acsodf

Article

Optimizing Dispersion of Silver Nanoparticle Incorporated Hydrogel Matrix by Silver Ion-Reducing Agent Self-Assembly

Tasawan Puttasakul, Pichai Sirisangwang, Nidcha Aroonrote, Chak Sangma,* and Wannisa Sukjee*

Cite This: *ACS Omega* 2025, 10, 62667−62674

Read Online

ACCESS | Metrics & More | Article Recommendations | Supporting Information

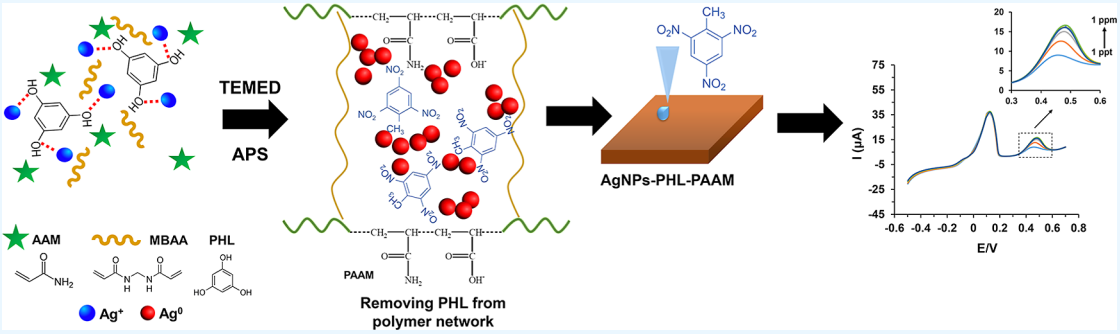

ABSTRACT: Nanoparticle-incorporated hydrogels are promising for functional material design, but effective dispersion of nanoparticles within the polymer matrix remains a critical challenge. This study presents a prepolymerization self-assembly strategy to optimize the distribution of silver nanoparticles (AgNPs) for sensing applications using phloroglucinol (PHL) as both a reducing agent and a self-assembly template. By inducing assembly between PHL and silver ions prior to polymerization, we achieved a uniform distribution of AgNPs throughout the hydrogel matrix. Characterization results confirmed the formation of a porous nanocomposite structure with superior stability. Crucially, electrochemical evaluations revealed that the hydrogel exhibits high specificity toward 2,4,6-trinitrotoluene (TNT). This selectivity is attributed to molecular recognition sites generated by the PHL-directed self-assembly. These findings offer a scalable approach to designing high-performance hydrogel sensors for the selective detection of explosives.

1. INTRODUCTION

The development of nanoparticle-incorporated hydrogels has advanced significantly in recent years,[1−3] providing new avenues for the fabrication of functional materials. A key component in measuring the efficacy of these materials is the self-assembly process, which generates intricate structures with distinct properties. For instance, researchers have utilized self-assembling nanocomposite hydrogels to create controlled-release drug delivery systems[4−6] and scaffolds for tissue engineering that mimic natural extracellular matrices to foster cell growth.[7−9] In the field of sensor technology, hydrogel self-assembly has been employed to construct responsive devices with enhanced detection capabilities.[10,11] The integration of self-assembly systems into hydrogels offers the potential to develop responsive systems with tunable properties. This versatility allows for the design of advanced materials in diverse fields, ranging from sensing and detection to soft robotics[12] and electromagnetic interference shielding,[13] where the controlled integration of micro- and nanoparticles is crucial for performance. These examples illustrate the versatility of self-assembly mechanisms across various scientific domains.

Silver nanoparticles (AgNPs) are of particular interest due to their unique optical, electrical, and catalytic properties.[14−16] Consequently, AgNP-directed self-assembly systems are increasingly embedded within polymeric frameworks,[17,18] such as hydrogels, to form nanocomposites. Hydrogels, which are three-dimensional networks of hydrophilic polymers, are capable of retaining significant water volumes. Integrating self-assembling AgNPs into these networks allows for the development of responsive systems with tunable properties suitable for advanced applications.[19−22]

Traditionally, the preparation of these composites involves three distinct steps: synthesizing AgNPs, mixing them with small molecules to induce self-assembly,[23] and subsequently incorporating this system into the hydrogel framework. However, optimizing the dispersion of AgNPs within the matrix remains a challenge. This work describes a synthesis strategy that integrates silver ions into the self-assembling system prior to

Received: July 16, 2025
Revised: November 30, 2025
Accepted: December 15, 2025
Published: December 18, 2025

nanoparticle formation, thereby engineering functional materials with highly dispersed AgNPs.

While various compounds serve as reducing agents in nanoparticle synthesis, the influence of the reducing agent's molecular structure on the hydrogel's final framework and functional properties is underexplored. Key questions remain regarding whether the reducing agent can impart specific structural features or recognition capabilities to the hydrogel. To address this, we introduce a synthesis method wherein phloroglucinol (PHL) acts as both a reducing agent and a self-assembling template for silver ions within a polyacrylamide hydrogel matrix. This study aims to elucidate the mechanism of AgNP-induced self-assembly and demonstrate its practical application in the selective electrochemical sensing of nitroaromatic explosives, specifically 2,4,6-trinitrotoluene (TNT). These findings contribute to the development of novel materials with tailored properties for specific functional applications.

2. EXPERIMENTAL SECTION

2.1. Materials. Acrylamide (AAM) monomer and phloroglucinol (PHL) were purchased from Merck. *N*,*N*′-Methylenebis(acrylamide) (MBAA), ammonium persulfate (APS), and picric acid were obtained from Sigma-Aldrich. Silver nitrate ($AgNO_3$) was sourced from CARLO ERBA reagents, and *N*,*N*,*N*′,*N*′-tetramethylethylenediamine (TEMED) was obtained from Bio-Rad. 2,4-Dinitrotoluene (DNT) was acquired from TCI Chemicals. Trinitrotoluene (TNT) and pentaerythritol tetranitrate (PETN) were provided by the Royal Thai Army. 4-Nitrophenol was purchased from Acros Organics. Distilled water was used as the solvent throughout the study.

2.2. Preparation of AgNP-Mediated Hydrogel. AAM monomer was mixed with MBAA cross-linker at a ratio of 29:1 (%w/w) in distilled water to prepare a 30% w/v AAM solution. Then, 300 μL of 20 mg/mL $AgNO_3$ solution was added to 1000 μL of the 30% AAM solution, followed by the addition of 20 mg of phloroglucinol. The mixture was stirred for 15 min. Polymerization was initiated by 10% w/v APS and catalyzed by TEMED. The solution color changed from colorless to yellow, after which it was transferred into an acrylic mold (3 mm thickness). After 15 min, the resulting silver nanoparticle-embedded polyacrylamide gel was solidified, removed from the mold, and cut into 1 cm^2 pieces. The gel was sonicated in 50 mL of distilled water for approximately 30 min to yield obtained AgNPs with cavities of occupation sites of phloroglucinol in polyacrylamide gel (AgNPs-PHL-PAAM). The final gel was soaked in distilled water prior to use. We used the hydrogel prepared from AgNP adding to acrylamide prepolymer (AgNPs-PAAM) without PHL served as a control material. Figure 1 illustrates the physical appearance of polyacrylamide hydrogels, including both AgNPs-PHL-PAAM and AgNPs-PAAM.

2.3. Characterization of the Hydrogels. Scanning electron microscope (SEM) analysis was performed to study the morphology of PAAM hydrogels. To prepare a sample for SEM analysis, the polyacrylamide hydrogels were soaked in distilled water before freeze-drying for a day to remove water while maintaining the pore structure within the gels. Briefly, the hydrogels were initially frozen at − 58 °C for 12 h, followed by freeze-drying under a vacuum pressure at 6 Pa for 24 h. The morphology of the PAAM hydrogels were investigated using the Quanta 450 SEM at the accelerating voltage of 10 kV.

The size, shape, and crystallinity of the synthesized AgNPs were characterized using field emission transmission electron microscopy (FE-TEM). The sample for TEM analysis was prepared dispersing 2 drops of the nanoparticle-containing hydrogel onto a copper grid, followed by drying at room temperature. Imaging was performed using a JEOL-JEM3100F microscope operated at an accelerating voltage of 300 kV. The crystalline structure of the AgNPs was confirmed by selected area electron diffraction (SAED).

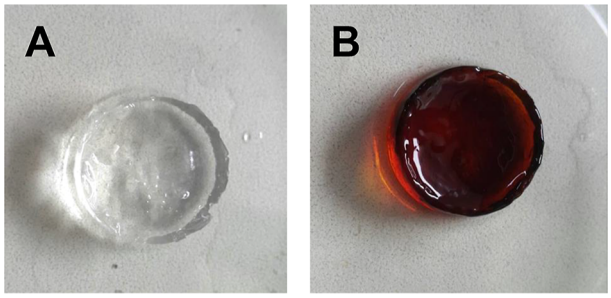

Figure 1. Appearance of polyacrylamide hydrogels (A) AgNPs-PAAM. (B) AgNPs-PHL-PAAM.

X-ray diffraction (XRD) analysis was performed to identify the crystalline phase of the AgNPs using a Bruker D8 Advance diffractometer. Diffraction patterns were recorded over a 2θ range of 30° to 80°. The AgNPs were initially embedded within the polyacrylamide hydrogel network. To isolate the nanoparticles, the polymer matrix was removed by thermal calcination at elevated temperature for 2 h. The crystal structure of the resulting silver powder was then characterized by XRD. Along with other experiments, XRD was another approach used to confirm the presence of silver in the hydrogel.[24] Here, the sample was calcinated at high temperature to make it feasible for XRD. It should be noted that sample preparation in this manner affected the structure and sizes of the nanoparticles[25] therefore other information besides the presence of silver cannot be obtained.

2.4. Electrochemical Measurement Procedure. Each electrochemical measurement was performed with the potentiostat (Autolab PGSTAT302N, Metrohm Siam, Thailand). First, the hydrogel (1 × 1 cm^2) was placed on a screen-printed electrode with gold as working and counter electrodes, and silver as the reference electrode (DRP-220BT, Metrohm Siam, Thailand). Then, the signals from phosphate buffered saline (PBS) and probe solutions were detected in cyclic voltammetry (CV) or linear sweep voltammetry (LSV) mode.

CV was used to evaluate the redox behavior of silver nanoparticles embedded within the hydrogel matrix by monitoring the oxidation and reduction peak currents and potentials, thereby providing insights into the electrochemical activity, stability, and electron transfer characteristics of the nanocomposite-modified electrode surface.

LSV mode was used to investigate the effect of selected oxidizing agents on AgNPs by monitoring the current of the silver oxidation peak. During each measurement, the electrical currents of AgNPs were recorded using a scan rate of 0.01 V/s within the range of −0.5 to 0.7 V. For each LSV experiment, the solutions of samples were prepared at concentrations of 1 ppt, 10 ppt, 100 ppt, 1 ppb, 10 ppb, 100 ppb, and 1 ppm for testing with the AgNPs-PAAM gel. Measurements were conducted on TNT and other samples, including DNT, PETN, picric acid, phloroglucinol, and 4-nitrophenol. In the experiment, the sample solution was dropped onto the AgNPs-PAAM gel and allowed to dry for approximately 2 min before performing LSV

https://doi.org/10.1021/acsomega.5c06979
ACS Omega 2025, 10, 62667−62674

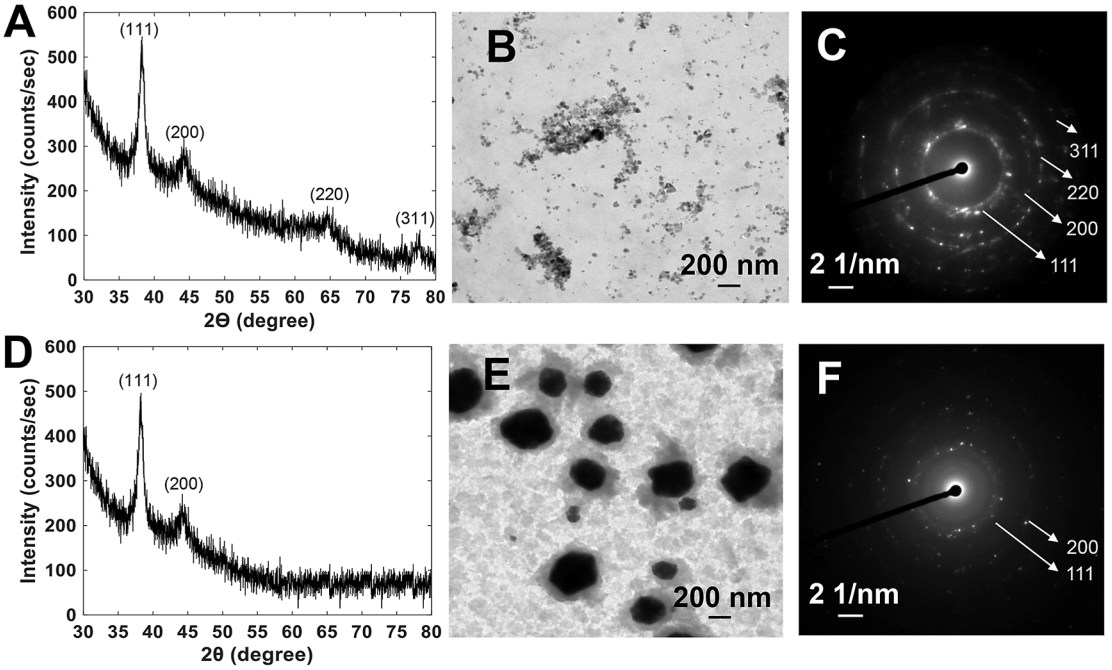

Figure 2. XRD pattern of AgNPs-PHL-PAAM and AgNPs-PAAM (A,D). Both systems exhibited AgNP characteristic planes and the TEM images (B,E). The XRDs from both systems had planes 111 and 200 in common but the pattern from AgNPs-PHL-PAAM showed more complicated patterns with additional 220 and 311 planes. This was confirmed by SAED pattern obtained for AgNPs-PHL-PAAM gels and AgNPs-PAAM (C,F).

measurements. Sample drop concentrations ranging from 1 ppt to 1 ppm were tested in triplicate for all experiments.

3. RESULT AND DISCUSSION

This study investigated how the self-assembly of Ag^+ ions with PHL prior to reduction affects the inclusion, dispersion, and properties of AgNPs within a polyacrylamide hydrogel. Characterization by XRD, SAED, TEM, and SEM confirmed that adding PHL to the prepolymeric mixture is transformative. It drives a self-assembly process that enhances AgNP incorporation into the hydrogel matrix, altering the nanoparticles' distribution, crystalline structure, and electrochemical properties.

3.1. Characterization of the AgNPs-PHL-PAAM. The hydrogel prepared without PHL (AgNPs-PAAM) was colorless, while the hydrogel prepared with PHL (AgNPs-PHL-PAAM) was dark brown, implying a higher concentration of AgNPs as depicted in Figure 1. The XRD pattern of AgNPs-PHL-PAAM gels confirmed the presence of crystallographic planes in AgNPs (Figure 2A), while for AgNPs-PAAM gels, the XRD pattern exhibited prominent peaks indexed to fewer planes of AgNPs as shown in Figure 2D. The TEM images indicated that AgNPs formed in the presence of PHL, AgNPs-PHL-PAAM, had smaller average sizes and highly distributed (Figure 2B) compared to those without PHL, AgNPs-PAAM (Figure 2E). A statistical analysis of the TEM images (Figure 3) quantified the significant impact of PHL on nanoparticle size and dispersion. The histogram clearly showed that AgNPs-PHL-PAAM exhibited a much narrower size distribution with diameters ranging from 4 to 10 nm. In contrast, a control AgNPs-PAAM gel displayed a broader size distribution with particle sizes ranging from 15 to 27 nm.

The SAED patterns exhibited distinct patterns for AgNPs-PHL-PAAM and AgNPs-PAAM gels which correlated with the

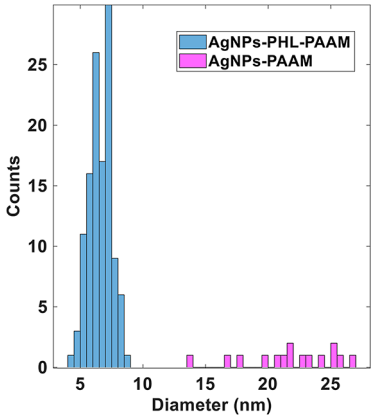

Figure 3. Size distribution histogram of AgNPs within hydrogels measured from TEM images. AgNPs-PHL-PAAM (blue bars) show a narrower and smaller particle size distribution, while AgNPs-PAAM (purple bars) display a broader distribution with larger particle sizes ranging from 15 to 27 nm.

XRD patterns but implied more complicated structures for AgNPs-PHL-PAAM as depicted in Figure 2C and F.

The SEM analysis of AgNPs-PHL-PAAM showed AgNPs clusters on both the gel cavity and external surface (Figure 4A,B) while AgNPs-PAAM hydrogel showed silver particles presented only on the gel surface (Figure 4C,D).

These results suggest that AgNPs-PHL-PAAM exhibited a more distributed silver presence and a smaller size inside the polymer matrix compared to AgNPs-PAAM, indicating successful incorporation of AgNPs to PAAM as depicted in Figure 5.

3.2. PHL Induced AgNPs Incorporation. AgNPs in PAAM hydrogels were prepared with and without PHL. Both preparations yielded AgNPs since AAM alone can serve as a reducing agent.[26] To optimize the synthesis of AgNPs, the

https://doi.org/10.1021/acsomega.5c06979
ACS Omega 2025, 10, 62667−62674

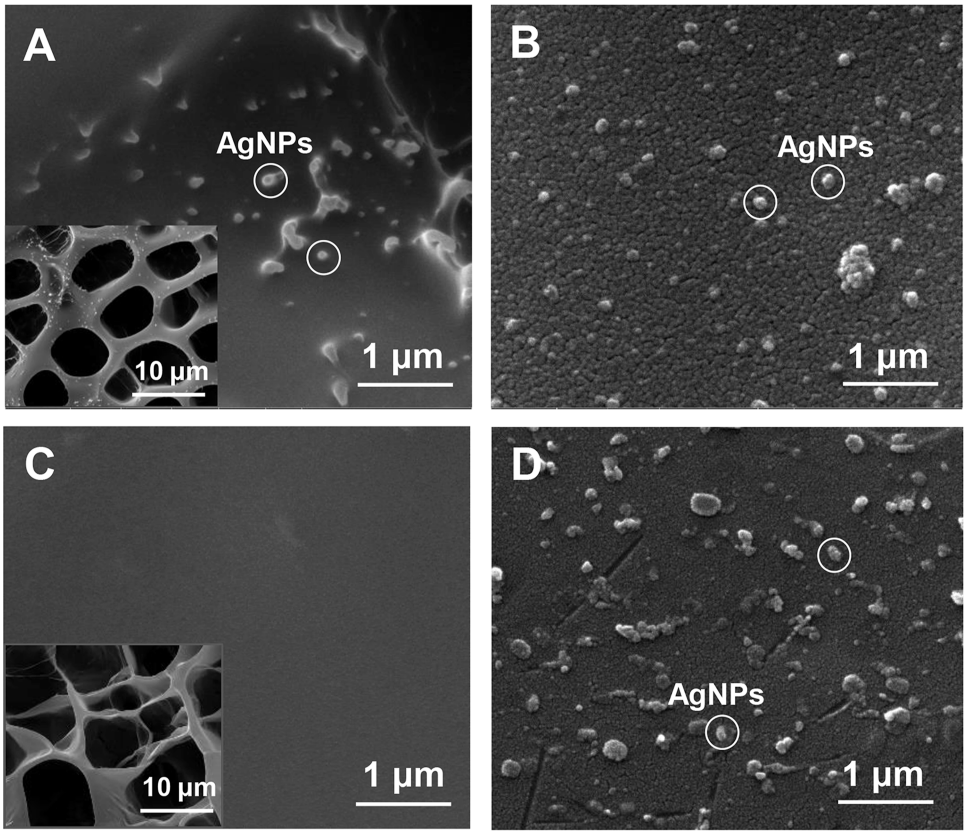

Figure 4. SEM images revealed a significant difference in the spatial distribution of AgNPs. The AgNPs-PHL-PAAM hydrogel showed nanoparticles dispersed throughout the entire matrix, located both deep within its porous interior (A) and across its surface (B). In contrast, the nanoparticles in the control AgNPs-PAAM gel are confined to the surface. They are found exclusively on the gel's exterior (D) and are completely absent from the interior (C).

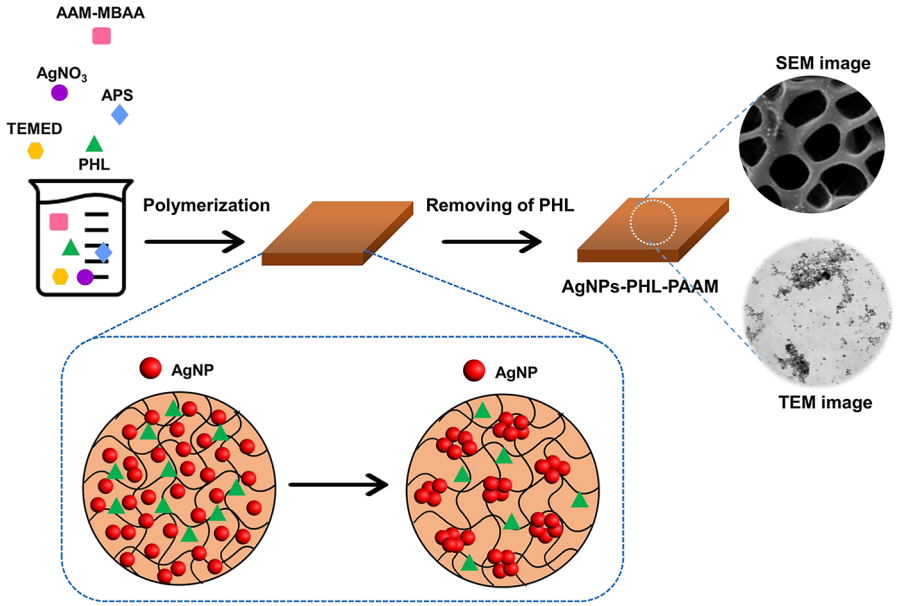

Figure 5. Depiction of the proposed AgNP self-assembly process in AgNPs-PHL-PAAM hydrogel as a result of PHL addition in prepolymeric mixture.

concentration of the reducing agent (PHL) was varied across 35, 55, and 80 mM. Experimental results revealed that the AgNP size distribution is inversely related to the PHL concentration (Figure S1). Specifically, lowering the PHL concentration facilitates the formation of larger particles, offering a degree of tunability for applications requiring different size ranges.

For the fabrication of the final composite material, the highest concentration of 80 mM was selected, corresponding to the aqueous solubility limit of PHL. Since the synthesis relies on PHL self-assembly, this saturation point effectively caps the minimum achievable particle size and total loading under current conditions. While this one-pot method is conducive to

https://doi.org/10.1021/acsomega.5c06979
ACS Omega 2025, 10, 62667−62674

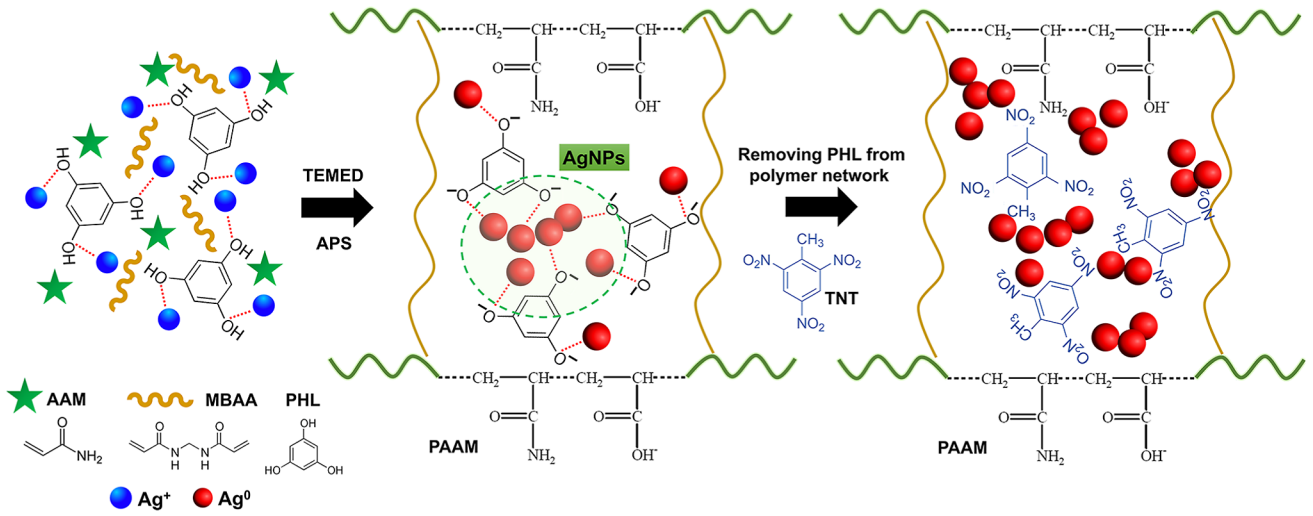

Figure 6. Schematic representation of AgNP formation within the AgNPs-PHL-PAAM hydrogel and the subsequent sensing mechanism. Ag^+ ions coordinate with PHL during polymerization (left), form AgNPs in situ (middle), and interact with TNT after PHL removal, all within the confined PAAM network (right).

scaling, future industrial applications requiring strictly defined particle sizes or higher loading might necessitate alternative reducing agents or cosolvents to overcome these solubility constraints.

Mechanistically, the reduction of silver ions by PHL likely proceeds via a proton-coupled electron transfer (PCET) pathway (Figure 6), which is characteristic of polyphenol oxidation.[27,28] Unlike simple reducing agents, PHL acts simultaneously as a reductant and a structural template. The synthesis begins with the coordination of Ag^+ to the oxygen atoms of the PHL hydroxyl groups. This hydroxyl triad allows PHL to chelate or weakly coordinate multiple Ag^+ ions, forming a prenucleation complex. Subsequently, the oxidation of PHL donates electrons to the silver ions, releasing protons and generating phloroglucinol radical species, while the reduced metallic silver (Ag^0) atoms aggregate to form stable nuclei.

Because the Ag^+ ions are precoordinated to the PHL scaffold, nucleation sites are spatially constrained. This confinement leads to smaller, more uniform nanoparticles (4−10 nm) compared to the larger, polydisperse particles (15−27 nm) formed by random reduction in the PAAM-only control (Figure 3). Notably, a PHL-to-silver nitrate molar ratio of 4.5:1 was employed. This approach deviates significantly from traditional methods where a 10 to 100-fold excess of the reducing agent is standard.[29,30] Nevertheless, this comparatively low ratio was sufficient to produce a stable AgNPs-PHL-PAAM hydrogel that exhibited excellent performance in detecting nitro-aromatic compounds.

3.3. PHL-AgNPs Self-Assembly. In addition to the differences in distribution and sizes of AgNPs, the AgNPs exhibited distinct electrochemical reaction profiles using CV. Subsequently, an electrochemical experiment was conducted using a set of probe molecules to induce electrochemical reactions with AgNPs.

The CV results from both hydrogels, AgNPs-PAAM and AgNPs-PHL-PAAM, showcased the characteristic peaks of AgNPs, affirming their presence. This is because the AAM in both systems has the capability to reduce Ag^+.[26] However, a deeper dive into the reaction profile of the AgNPs against selected compounds unveiled distinct behaviors (Figure 7). First, the small peak at 0.45 V implied that AgNP clusters of AgNPs-PHL-PAAM hydrogel existed smaller AgNP particle size[31] which related to the TEM analysis (Figure 2B and E).

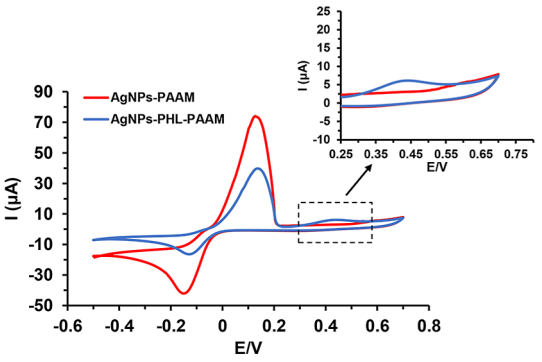

Figure 7. CV scan of AgNPs-PHL-PAAM hydrogel demonstrates two oxidation peaks at 0.12 and 0.45 V as compared to a single peak from CV of AgNPs-PAAM.

To evaluate the hydrogel's performance, we compared the electrochemical response of the AgNPs-PHL-PAAM hydrogel against a control AgNPs-PAAM gel using LSV (Figure 8A,B). Our analysis focused on the electrical current shift at 0.45 V, a signal generated from the oxidation of AgNPs by interaction with the target molecules.

The results for the AgNPs-PHL-PAAM hydrogel were uniquely distinguished. Intriguingly, its LSV graph displayed two distinct oxidation peaks at 0.12 and 0.45 V, the peak at 0.45 V was completely absent in the control gel showing only minor current changes from 0.71 to 1.44 μA (Figure 8B inset). The first peak (0.12 V) likely corresponds to the oxidation of Ag^0 to Ag^+, while the second, crucial peak (0.45 V) may represent further oxidation of Ag^+ or effects from small AgNP clusters (Figure 8A). A comparative study was conducted at 0.12 V to evaluate the response of the AgNPs-PHL-PAAM hydrogel versus a control hydrogel when exposed to TNT and other nitro-compounds. The resulting current was found to be the same for both materials in the presence of all tested compounds (Figure S2), demonstrating a lack of selectivity at this potential.

https://doi.org/10.1021/acsomega.5c06979
ACS Omega 2025, 10, 62667−62674

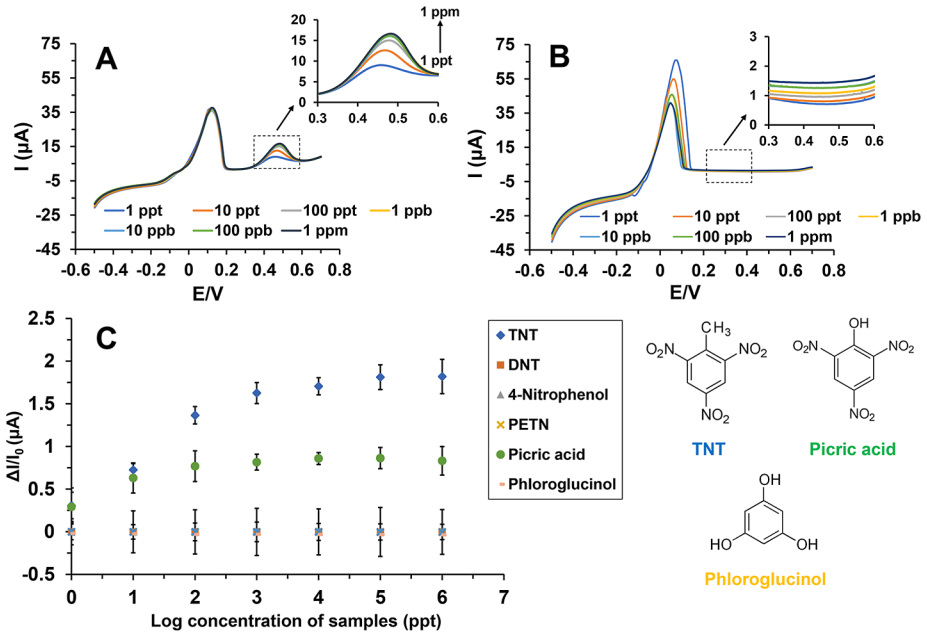

Figure 8. Electrical current response to TNT (from 1 ppt to 1 ppm) was measured using LSV with a scan rate of 0.01 V/s over a potential range of −0.5 to 0.7 V. The 0.45 V peak from AgNPs-PHL-PAAM (A) LSV increased with TNT concentration while the peak at 0.12 V remained unchanged. The AgNPs-PAAM gel responded to TNT (B) with the decrease in signal at 0.12 V and no signal changes observed with TNT. Comparison of the current responses at 0.45 V from AgNPs-PHL-PAAM hydrogel toward TNT and other nitroaromatic compounds, demonstrating high selectivity for TNT detection (C).

However, the basis for selective detection is the distinct electrochemical peak observed at 0.45 V.

Comparative electrochemical testing reveals that the specific oxidation peak at 0.45 V, crucial for the selective detection of nitroaromatic compounds is exclusively present in the uniform AgNPs-PHL-PAAM system (Figure 8A). In contrast, the nonuniform control (AgNPs-PAAM, containing larger 15−27 nm particles) completely failed to exhibit this peak (Figure 8B). This demonstrates that sensing functionality is not merely intrinsic to silver but depends strictly on the uniform, small-cluster architecture enabled by PHL, which maximizes accessible binding sites and prevents the aggregation observed in the control.

As shown in Figure 8C, the electrochemical response of the AgNPs-PHL-PAAM hydrogel exhibits distinct selectivity. For the trinitro-aromatic compounds TNT and picric acid, the oxidation current at 0.45 V demonstrates a clear concentration dependence, increasing linearly with the logarithm of the sample concentration from 1 ppt to 1 ppm. In stark contrast, structurally related compounds with fewer nitro groups, specifically DNT, 4-nitrophenol, and PETN, exhibited concentration independence, with the current response remaining negligible and unchanged across the tested concentration range. This confirms the sensor's high selectivity toward electron-deficient trinitro-aromatic species.

The distinct electrochemical behavior of the AgNPs-PHL-PAAM hydrogel can be attributed to a molecular recognition mechanism driven by the structural similarity between the templating agent (PHL) and the target analytes. PHL is a trihydroxybenzene derivative with high symmetry. During the self-assembly and reduction process, PHL acts as a molecular template, creating recognition sites or cavities on the AgNP surface or within the hydrogel matrix that match its specific geometry and electronic distribution. TNT and picric acid are trinitro-aromatic compounds. They share the same benzene ring core and a similar symmetric arrangement of functional groups (three nitro groups) as the PHL template. This molecular recognition allows them to bind effectively to the binding sites, facilitating the electrochemical oxidation at 0.45 V. Consequently, as the concentration of these matching analytes increases, more sites are occupied, and the current rises. Conversely, DNT and 4-nitrophenol lack the requisite three functional groups, and PETN lacks the aromatic ring entirely. Because they are structurally dissimilar to the PHL template, they cannot fit into the molecular recognition sites and therefore do not trigger the specific electrochemical response, resulting in a low, constant signal regardless of concentration. This is particularly compelling as we did not observe any selective reduction of nitro aromatic compounds from the AgNPs-PAAM control hydrogel. To evaluate the reliability of the fabrication process, sensor-to-sensor reproducibility was assessed by testing three independently prepared AgNPs-PHL-PAAM hydrogels against 10 ppt TNT. The measurements yielded an average current response of 0.72 ± 0.07 μA, resulting in a relative standard deviation (RSD) of 9.72%, which indicates satisfactory consistency in the synthesis and sensing performance.

4. CONCLUSIONS

This study demonstrates that adding PHL during the synthesis of AgNPs-PHL-PAAM hydrogel results in smaller, more evenly distributed AgNPs within the polymer matrix. The resulting AgNPs-PHL-PAAM hydrogel exhibits a distinct electrochemical response, showing a specific electrical current increase at 0.45 V when exposed to trinitroaromatic compounds like TNT and picric acid. This selective detection is not observed in hydrogels prepared without PHL. The findings suggest that PHL self-assembles within the hydrogel, creating recognition sites that are structurally similar to these nitroaromatic compounds, thereby enabling specific detection. This work highlights a method for

https://doi.org/10.1021/acsomega.5c06979
ACS Omega 2025, 10, 62667−62674

developing functional materials with tailored electrochemical properties for sensor applications.

These findings have practical implications for the development of electrochemical sensors capable of detecting trace levels of explosive residues or environmental contaminants. The AgNPs-PHL-PAAM hydrogel could be integrated into low-cost, portable sensing platforms for use in security screening, environmental monitoring, or forensic analysis.

Future research should explore alternative reducing or stabilizing agents to enhance the hydrogel's properties. Crucially, the focus must shift toward device engineering: specifically, optimizing the hydrogel−transducer interface and adapting the synthesis for compatible fabrication methods to ensure robust performance in real-world applications.

■ ASSOCIATED CONTENT

Supporting Information

The Supporting Information is available free of charge at https://pubs.acs.org/doi/10.1021/acsomega.5c06979.

TEM image of AgNPs with different amounts of reducing agents and current responses at 0.12 V for various nitro compounds at different concentrations of AgNPs-PHL-PAAM and AgNPs-PAAM hydrogels (PDF) (PDF)

■ AUTHOR INFORMATION

Corresponding Authors

Chak Sangma − *Department of Chemistry, Faculty of Science and Center for Advanced Studies in Nanotechnology for Chemical, Food and Agricultural Industries, Kasetsart University, Bangkok 10900, Thailand;* orcid.org/0000-0002-2627-8073; Email: fscicsm@ku.ac.th

Wannisa Sukjee − *Department of Chemistry, Faculty of Science and Center for Advanced Studies in Nanotechnology for Chemical, Food and Agricultural Industries, Kasetsart University, Bangkok 10900, Thailand; Advanced Porous Materials for One Health Integrations (APM Unit), Special Research Incubator Unit, Kasetsart University, Bangkok 10900, Thailand;* orcid.org/0000-0003-1250-0451; Email: fsciwisu@ku.ac.th

Authors

Tasawan Puttasakul − *College of Biomedical Engineering, Rangsit University, Pathumthani 12000, Thailand*

Pichai Sirisangwang − *Science Equipment Center, Faculty of Science, Kasetsart University, Bangkok 10900, Thailand*

Nidcha Aroonrote − *Center for Advanced Studies in Nanotechnology for Chemical, Food and Agricultural Industries, Kasetsart University, Bangkok 10900, Thailand*

Complete contact information is available at: https://pubs.acs.org/10.1021/acsomega.5c06979

Author Contributions

T.P, W.S, and C.S. conceived and planned the experiments. T.P carried out the experiments. T.P and W.S. contributed to sample preparation. T.P, W.S, and C.S. contributed to the interpretation of the results. T.P. took the lead in writing the manuscript. C.S, W.S edit and review the manuscript. P.S and N.A assisted with SEM imaging. All authors provided critical feedback and helped shape the research, analysis and manuscript.

Notes

The authors declare no competing financial interest.

■ ACKNOWLEDGMENTS

The authors would like to thank the Royal Thai Army (RTA) for providing the explosive materials used in this work. This work was supported by Kasetsart University Research and Development Institute (KURDI, grant number: YF(KU)21.67 and FF(KU-SRIU)11.67), Kasetsart University and National Research Council of Thailand (NRCT, Grant number: N41A640073), Chulalongkorn University.

■ REFERENCES

(1) Zhang, S.; Ou, Q.; Xin, P.; Yuan, Q.; Wang, Y.; Wu, J. Polydopamine/puerarin nanoparticle-incorporated hybrid hydrogels for enhanced wound healing. *Biomater. Sci.* **2019**, *7* (10), 4230−4236.

(2) Chakraborty, A.; Roy, A.; Ravi, S. P.; Paul, A. Exploiting the role of nanoparticles for use in hydrogel-based bioprinting applications: concept, design, and recent advances. *Biomater. Sci.* **2021**, *9* (19), 6337−6354.

(3) Derakhshankhah, H.; Eskandani, M.; Akbari Nakhjavani, S.; Tasoglu, S.; Vandghanooni, S.; Jaymand, M. Electro-conductive silica nanoparticles-incorporated hydrogel based on alginate as a biomimetic scaffold for bone tissue engineering application. *Int J Polym Mater* **2024**, *73* (4), 266−278.

(4) Chen, K.; Zhang, Y.; Zhu, L.; Chu, H.; Shao, X.; Asakiya, C.; Huang, K.; Xu, W. Insights into nucleic acid-based self-assembling nanocarriers for targeted drug delivery and controlled drug release. *J. Controlled Release* **2022**, *341*, 869−891.

(5) Li, X.; Liu, H.; Yu, A.; Lin, D.; Bao, Z.; Wang, Y.; Li, X. Bioinspired self-assembly supramolecular hydrogel for ocular drug delivery. *Chin. Chem. Lett.* **2021**, *32* (12), 3936−3939.

(6) Li, T.; Shi, C.; Mi, Z.; Xu, H.; Xu, J.; Wang, L.; Zhang, X. Biocompatible puerarin injectable-hydrogel using self-assembly tetrapeptide for local treatment of osteoarthritis in rats. *J. Drug Delivery Sci. Technol.* **2022**, *78*, 103909.

(7) Appel, E. A.; Tibbitt, M. W.; Webber, M. J.; Mattix, B. A.; Veiseh, O.; Langer, R. Self-assembled hydrogels utilizing polymer−nanoparticle interactions. *Nat. Commun.* **2015**, *6* (1), 6295.

(8) Auvinen, V.-V.; Laurén, P.; Shen, B.; Isokuortti, J.; Durandin, N.; Lajunen, T.; Linko, V.; Laaksonen, T. Nanoparticle release from anionic nanocellulose hydrogel matrix. *Cellulose* **2022**, *29* (18), 9707−9717.

(9) Pek, Y. S.; Wan, A. C. A.; Shekaran, A.; Zhuo, L.; Ying, J. Y. A thixotropic nanocomposite gel for three-dimensional cell culture. *Nat. Nanotechnol.* **2008**, *3* (11), 671−675.

(10) Puttasakul, T.; Tancharoen, C.; Sukjee, W.; Sangma, C. Vapor-Phase Substrate Nitroreductase Reaction and Its Application as TNT Electrochemical Gas Sensor. *IEEE Sens. J* **2022**, *22* (23), 22368−22373.

(11) Hu, C.; Zhai, X.; Liu, L.; Zhao, Y.; Jiang, L.; Qu, L. Spontaneous Reduction and Assembly of Graphene oxide into Three-Dimensional Graphene Network on Arbitrary Conductive Substrates. *Sci. Rep.* **2013**, *3* (1), 2065.

(12) Li, J.; Miao, J.; Tsang, A. C. H. Self-regulated photoresponsive heterogeneous PNIPAM hydrogel actuators. *Nanoscale* **2025**, *17* (27), 16230−16238.

(13) Yan, Q.; Liu, Z.; Xiong, J.; Lian, H.; Chen, H.; Fei, T.; Chen, Y.; Zheng, H.; Zhao, X.; Xu, L.; Xue, F.; Zhong, Y.; Ma, X.; Shi, L.; Peng, Q.; He, X. Stimuli-Responsive MXene/PNIPAM Hydrogel WITH High-Performance and Tunable Electromagnetic Interference Shielding Performance. *Adv. Sci. (Weinh.)* **2025**, *12* (31), No. e05551.

(14) Ali, I.; Imkan; Ikram, F.; Ahmad, F.; Nisar, J.; Shah, M. R.; Ali, S.; ullah, S.; Althagafi, I. I.; Ateeq, M. Sensing Applications of Triazole Conjugated Silver Nanoparticles. *J. Mol. Struct.* **2021**, *1226*, 129306.

(15) Modrzejewska-Sikorska, A.; Konował, E. Silver and gold nanoparticles as chemical probes of the presence of heavy metal ions. *J. Mol. Liq.* **2020**, *302*, 112559.

(16) Quadrado, R. F. N.; Gohlke, G.; Oliboni, R. S.; Smaniotto, A.; Fajardo, A. R. Hybrid hydrogels containing one-step biosynthesized silver nanoparticles: Preparation, characterization and catalytic application. *J. Ind. Eng. Chem.* **2019**, *79*, 326−337.

(17) Caillosse, E.; Zaier, M.; Mezghani, M.; Hajjar-Garreau, S.; Vidal, L.; Lougnot, D.; Balan, L. Photo-Induced Self-Assembly of Silver Nanoparticles for Rapid Generation of First and Second Surface Mirrors. *ACS Appl. Nano Mater.* **2020**, *3* (7), 6531−6540.
(18) Panigrahi, S.; Praharaj, S.; Basu, S.; Ghosh, S. K.; Jana, S.; Pande, S.; Vo-Dinh, T.; Jiang, H.; Pal, T. Self-Assembly of Silver Nanoparticles: Synthesis, Stabilization, Optical Properties, and Application in Surface-Enhanced Raman Scattering. *J. Phys. Chem. B* **2006**, *110* (27), 13436−13444.
(19) Ma, Y.; Shi, L.; Liu, F.; Zhang, Y.; Pang, Y.; Shen, X. Self-assembled thixotropic silver cluster hydrogel for anticancer drug release. *Chem. Eng. J.* **2019**, *362*, 650−657.
(20) Liu, S.; Yan, Q.; Cao, S.; Wang, L.; Luo, S.-H.; Lv, M. Inhibition of Bacteria In Vitro and In Vivo by Self-Assembled DNA-Silver Nanocluster Structures. *ACS Appl. Mater. Interfaces* **2022**, *14* (37), 41809−41818.
(21) Sukjee, W.; Sangma, C.; Lieberzeit, P. A.; Ketsuwan, K.; Thepparit, C.; Chailapakul, O.; Ngamrojanavanich, N. EV71 virus induced silver nanoparticles self-assembly in polymer composites with an application as virus biosensor. *Sens. Actuators, B* **2023**, *393*, 134324.
(22) Hou, C.; Ma, K.; Jiao, T.; Xing, R.; Li, K.; Zhou, J.; Zhang, L. Preparation and dye removal capacities of porous silver nanoparticle-containing composite hydrogels via poly(acrylic acid) and silver ions. *RSC Adv.* **2016**, *6* (112), 110799−110807.
(23) Szuwarzyński, M.; Mazur, Ł.; Borkowski, M.; Maćkosz, K.; Giżyński, K.; Mazur, T. Enhanced Assembly of Ag Nanoparticles for Surface-Independent Fabrication of Conductive Patterns. *ACS Appl. Nano Mater.* **2022**, *5* (9), 12711−12719.
(24) Guo, C.; Shao, F.; Zhang, Y.; Sheng, X.; Dong, Y. Preparation of silver/hydroxyapatite nanoparticles using hydroxyapatite nanoparticles with different calcination temperatures. *Nano-Micro Lett* **2012**, *7* (9), 904−906.
(25) Rad, M. S.; Kompany, A.; Zak, A. K.; Abrishami, M. E. The effect of silver concentration and calcination temperature on structural and optical properties of ZnO:Ag nanoparticles. *Mod. Phys. Lett. B* **2015**, *29* (01), 1450254.
(26) Salaheldin, H. I.; Almalki, M. H. K.; Hezma, A. E. M.; Osman, G. E. H. Facile synthesis of silver nanoparticles mediated by polyacrylamide-reduction approach to antibacterial application. *IET Nanobiotechnol* **2017**, *11* (4), 448−453.
(27) Irebo, T.; Reece, S. Y.; Sjödin, M.; Nocera, D. G.; Hammarström, L. Proton-Coupled Electron Transfer of Tyrosine Oxidation: Buffer Dependence and Parallel Mechanisms. *J. Am. Chem. Soc.* **2007**, *129* (50), 15462−15464.
(28) Zhang, D.; Wang, C.; Shen, L.; Shin, H.-C.; Lee, K. B.; Ji, B. Comparative analysis of oxidative mechanisms of phloroglucinol and dieckol by electrochemical, spectroscopic, cellular and computational methods. *RSC Adv.* **2018**, *8* (4), 1963−1972.
(29) Rivero, P. J.; Goicoechea, J.; Urrutia, A.; Arregui, F. J. Effect of both protective and reducing agents in the synthesis of multicolor silver nanoparticles. *Nanoscale Res. Lett.* **2013**, *8* (1), 101.
(30) Besenhard, M. O.; Baber, R.; LaGrow, A. P.; Mazzei, L.; Thanh, N. T. K.; Gavriilidis, A. New insight into the effect of mass transfer on the synthesis of silver and gold nanoparticles. *CrystEngComm* **2018**, *20* (44), 7082−7093.
(31) Chen, W.; Wang, H.; Tang, H.; Yang, C.; Li, Y. Unique Voltammetry of Silver Nanoparticles: From Single Particle to Aggregates. *Anal. Chem.* **2019**, *91* (22), 14188−14191.

https://doi.org/10.1021/acsomega.5c06979
ACS Omega 2025, 10, 62667−62674